PNAS
www.pnas.org

Main Manuscript for

Role of dynamic bonds on fatigue threshold of tough hydrogels

Xueyu Li[1] and Jian Ping Gong[1,2,*]

[1]Laboratory of Soft & Wet Matter, Faculty of Advanced Life Science, Hokkaido University, Kita 21, Nishi 11, Kita-ku, Sapporo 001-0021, Japan

[2]Institute for Chemical Reaction Design and Discovery (WPI-ICReDD), Hokkaido University, Kita 21, Nishi 11, Kita-ku, Sapporo 001-0021, Japan

*Jian Ping Gong

Email: gong@sci.hokudai.ac.jp

Author Contributions： X.L. designed and performed the experiments; X.L. and J.P.G. analysis the data and wrote the paper.

Competing Interest Statement: The authors declare no competing interest.

Classification： Physical Sciences, Applied Physical Sciences

Keywords： Fatigue threshold, dynamic bond, viscoelasticity, time–salt superposition, rate dependence

This PDF file includes:

Abstract

Fatigue threshold (G_0) is the energy release rate below which no fatigue crack advances. Understanding the relationship between the static/dynamic structures and G_0 of viscoelastic hydrogels is crucial for designing materials exposed to cyclic loading. In this study, we elaborate the role of dynamic bonds in the G_0 of tough hydrogels. Using polyampholyte hydrogels possessing abundant ionic dynamic bonds, we can adopt time–salt superposition principle to access a wide range of time scales that are difficult to access in fatigue test. G_0 was found rate-independent in the elastic regime at a low cyclic strain rate, whereas weak power-law relations between G_0 and strain rate were firstly observed in viscoelastic regimes. The former agrees with molecular explanation of Lake-Thomas model, and the latter is related to the self-healing property of dynamic bonds in viscoelastic regime that protects the permanent bonds from breaking. This work modifies the previous consideration that the dynamic bonds only contribute to the fracture toughness and crack resistance but not to the G_0.

Significance

Dynamic bonds have been found to enhance fracture toughness of hydrogels as sacrificial bonds. Whereas, the role of dynamic bonds to fatigue threshold of hydrogels is poorly understood because the wide dynamic range of viscoelastic response imposes a challenge on fatigue experiment. Here, by using polyampholyte hydrogels, we adopted time–salt superposition principle to access a wide range of time scales that are otherwise difficult to access in fatigue test. Relations between fatigue threshold and strain rate in elastic and viscoelastic regimes, and the corresponding mechanism correlated to permanent/dynamic

bonds were revealed. We believe that this work gives important insight into the design and development of fatigue-resistant soft materials composed of dynamic bonds.

Introduction

Viscoelasticity, derived from noncovalent/reversible interactions in covalent polymer networks, is a phenomenon commonly observed in soft materials, such as elastomers (1-4), hydrogels (5-7) and human tissues (8, 9). Viscoelastic dissipation associated with the rheological response of these noncovalent/reversible interactions plays an essential role in the toughness enhancement and crack resistance. Moreover, crack advancement in the cyclic fatigue test is also found correlated to the rheological response (10-12). However, whether the viscoelasticity plays roles on the fatigue threshold (G_0) for vanishing crack advancing velocities is still an open question.

Studies by Lake and coworkers on rubbers (12, 13) and Suo et al. on hydrogels (10, 11, 14) suggested G_0 is determined by the covalent network, whereas the noncovalent/reversible interactions make negligible contributions. These studies found that G_0 agrees quantitatively well with the Lake–Thomas model (13), which is interpreted by the scission of covalent bonds of the polymer chain lying across the crack plane. Conversely, the G_0 values of some viscoelastic soft materials do not quantitatively obey the Lake–Thomas model (15, 16). For example, polyampholyte hydrogels (PA gels) composed of a permanent crosslinking network and dynamic ionic bonds show a stronger relationship between G_0 and the mesh size of the permanent network than the scaling relation deduced from the Lake–Thomas model (15). We consider that these discrepancies in the viscoelastic effects might arise from different deformation rates of the fatigue test in

respective to the characteristic relaxation times of the viscoelastic materials. However, exploring the fatigue behaviors of the viscoelastic materials over a wide range of strain rates from elastic regime to viscoelastic regime is experimentally challenging.

In this work, we study the strain-rate dependence of G_0 of viscoelastic hydrogels with ionic bonds. The time–salt superposition principle allows us to tune the dynamics of the ionic bonds and thereby experimentally access a wide range of time scales for fatigue observation at a constant temperature. We show that G_0 increases weakly with strain rate in power-law relations in the viscoelastic regime. At the low-frequency limit of the pure elastic regime, where the dynamic bonds are turned off, G_0 becomes rate-independent, which can be explained by the Lake–Thomas model. We will discuss possible mechanism for the role of dynamic bonds on G_0 in the viscoelastic regimes. This work provides new insight into the relationship between viscoelastic response and fatigue resistance.

Results and Discussion

We adopted covalently crosslinked polyampholyte hydrogels (PA gels) as model materials. The PA gels carry equal positive and negative charges that are randomly distributed on the polymer network (**Fig. 1**). PA gels are dually crosslinked with permanent crosslinking by covalent crosslinkers and trapped entanglements, and dynamic crosslinking by ionic bonds between opposite charges on the polymer chains (6, 17, 18). The permanent crosslinking density could be tuned by the chemical crosslinker density and monomer concentration for the sample synthesis, whereas the dynamic crosslinking could be switched on and off by equilibrating the synthesized samples in pure water and in high ionic strength media, respectively. This is because salt ions screen electrostatic interactions

(19, 20), thereby accelerating the dynamics of ionic bonds between opposite charges on the polymer network. In this study, we adopted two sets of samples with different permanent crosslinks: a soft (PA-s) loosely crosslinked and a hard (PA-h) densely crosslinked (see details in *Materials and Methods section* and **Table 1**). The two sets of PA gels were studied in two different states: one was in the as-prepared state, before removing the small counter-ions (Na^+ and Cl^-) after synthesis; another was in the water-equilibrated state, after removal of the small ions by dialyzing the gels in water (**Fig. 1**). The salt-containing gels (as-prepared gels) only showed weak viscoelasticity because of the Debye screening effect of ionic bonds, whereas the salt-free gels (water-equilibrated gels) showed strong viscoelasticity owing to the formation of ionic bonds (**Figs. 2*A*** and **2*C***).

Analogous to time–temperature superposition (21) and strain-rate–frequency superposition (22), time–salt superposition is an approach to equivalently probe the rheological behavior of polyelectrolyte complexes at different time scales by varying the salt in the samples at a constant temperature (23, 24). This is because salt accelerates the dissociation processes of ionic bonds, which is equivalent to prolong the observation time scale for salt-free samples, and therefore reduces viscoelastic dissipation from ionic bonds. Therefore, the dynamic modulus curve $G_{salt}(\omega)$ of salt-containing PA gels at angular frequency ω is equivalent to the curve $G(\omega)$ of salt-free PA gels at $a_{salt}\omega$:

$$G(\omega) = b_{salt}G_{salt}(a_{salt}\omega) \quad (1)$$

The shift factor a_{salt} is determined by superimposing the $G_{salt}(\omega)$ curve on the $G(\omega)$ curve of salt-free PA gels. The modulus shift factor was $b_{salt} = \lambda_s^3$ due to polymer density difference in per unit volume, where λ_s^3 is the volume ratio of the salt-containing PA gels relative to salt-free PA gels.

Figs. 2*B* and **2*D*** shows the master curves $G(\omega)$ for salt-free PA gels at 24 °C by properly shifting the log-log $G(\omega)$–frequency curves of the salt-containing gels to match the curves of the salt-free gels (**Figs. 2*A*** and **2*C***). The shift factors used to rescale the as-prepared samples are listed in **Table 2**. This method allowed us to observe the dynamics of PA gels in a wide frequency range that are otherwise inaccessible under a constant temperature. The plateau regime at low frequency side is from the permanent crosslinking where the ionic bonds do not play a role. The increase of storage modulus (G') at high frequency roughly follows $G' \sim (a_{salt}\omega)^{0.5}$, and can be attributed to the sticky Rouse motion of associating polymer strands derived from ionic bonds (25). G' does not reach the plateau modulus at the high frequency limit, indicating that the lifetime of ionic bonds (τ_s) is short, beyond our observation window ($\tau_s < 10^{-5}$ s). From **Figs. 2*B*** and **2*D***, we can read the transition angular frequency from plateau regime to the viscoelastic regime as $\omega_v = 0.54$ and 0.15 rad/s for PA-s and PA-h, respectively. The ω_v could be related to the sticky Rouse time of associating polymer strands $\tau_v = \omega_v^{-1} = \tau_s(M_{eff}/M_s)^2$, where M_{eff} and M_s are the molecular mass of strands between neighboring effective permanent crosslinking points and between neighboring dynamic bonds ($M_{eff}>M_s$), respectively (25, 26). The very broad viscoelastic regime of PA gels could be attributed to the small M_s due to high density of dynamic bonds on the strands. Closer inspection of the master curves reveals differences between the moduli at low frequencies. The G' for PA-h is independent of frequency and much larger than loss modulus (G'') with tan δ on the order of 0.02. As a comparison, the G' of PA-s has a weak frequency dependence at low frequencies, and tan δ is larger than that of PA-h. The latter is a feature of imperfect networks owing to the gradual relaxation

of imperfect structures, such as dangling structures (27). From the plateau modulus G' at the low-frequency limit, the effective permanent cross-linking densities were estimated as $\nu_e = 2.1\times10^{24}$ and 1.7×10^{25} m^{-3}, and the number of monomers per network strand are $N_{x,eff}$ = 1080 and 130, for PA-s and PA-h, respectively (see *Materials and Methods section*, **Table 1**). The effective permanent crosslinking results from both chemical crosslinking and entrapped entanglements in this PA system, as we have demonstrated that physically trapped entanglements act similarly as chemical crosslinks to control the fatigue threshold, i.e., a higher concentration of trapped entanglements induces a lower fatigue threshold (15). But for the chemical crosslinking hydrogels without dynamic bonds, the fracture energy and fatigue threshold can be improved by entanglements, as suggested by Suo et al.(28) and Zhao et al.(29). As the weakly crosslinked PA-s still does not reach the plateau modulus at the low frequency limit, the estimated $N_{x,eff}$ might be slightly lower than the true value. Also, the ω_v of PA-s represents the critical frequency entering the strongly viscoelastic region.

Next, we study the fracture behaviors under nominal strain rates $\dot{\varepsilon} = v/H_0 = 0.25$ and 2.5 s^{-1}, where v is the loading speed and H_0 is the sample height when undeformed. The corresponding measurement positions in the dynamic spectra are indicated by vertical dotted lines in **Fig. 2*B*** and **2*D*** for PA-s and PA-h, respectively. In the following sections, we use the dimensionless quantity, $D_i = 2\pi a_{salt}\dot{\varepsilon}/\omega_v$, to denote the observation regime. $D_i > 1$ corresponds to the viscoelastic regime, and $D_i < 1$ corresponds to the elastic regime. Owing to the time–salt superposition, the two strain rates $\dot{\varepsilon}$ = 0.25 and 2.5 s^{-1} used in the measurements correspond to a wide dynamic range from the elastic regime ($D_i \sim 10^{-2}$) to

viscoelastic regime ($D_i \sim 10^2$). Because PA-s exhibits a slight frequency dependence even in the low-frequency limit, weak viscoelasticity may exist even in the low strain rate limit.

Fracture energy was measured using a pure shear test (30-32). The pre-notched sample was stretched to fracture, and the critical stretch ratio at which the crack propagation started was denoted as λ_c (**Fig. 2*E*** and *SI Appendix*, **Fig. S1**). The fracture energy is calculated from $\Gamma = W(\lambda_c)H_0$, where $W(\lambda_c)$ is the energy density of the unnotched sample stretched to λ_c. To compare the mechanical properties of the gels in the same state, the Γ and the energy release rate (G) in the following discussion are rescaled by the area swelling ratio λ_s^2 to correct the chain density per unit area. **Fig. 2*F*** shows that the rescaled fracture energy ($\lambda_s^2\Gamma$) increases with $D_i = 2\pi a_{salt}\dot{\varepsilon}/\omega_v$, following power law relations $\lambda_s^2\Gamma \sim (D_i)^{\alpha}$, where $\alpha = 0.27$ and 0.28 for PA-s and PA-h, respectively. This scaling exponent is consistent with the previously reported value for PA gels in the viscoelastic regime ($\alpha = 0.21$) (33). We notice that this scaling relation holds for a wide strain rate range from the elastic regime to the viscoelastic regime. This result indicates that even the remote deformation is in the elastic regime, complex viscoelastic energy dissipation is involved in the crack advancement.

Next, we investigated the effect of strain rate on the fatigue threshold G_0, following our previous method (34). We performed cyclic fatigue test under the nominal strain rates $\dot{\varepsilon} =$ 0.25 and 2.5 s^{-1} using the pure shear geometry shown in **Fig. 2*E***. The maximum and minimum stretch ratios at each cycle were maintained at the preset values of λ_{max} and 1, respectively. Note that the time–salt superposition approach extends the observation time scale of fatigue test over four decades in strain rate at room temperature (D_i decreases from 10^2 to 10^{-2}), otherwise, one complete fatigue test at a low strain rate would take more than

6 years. During cyclic loading, we used a high-resolution digital camera (pixel size ~ 15 μm) for tracking the crack growth of the pre-notched samples, and the crack growth length was denoted as c. The fatigue crack growth per cycle ($\Delta c/\Delta N$) can be obtained from the fitting slope of c in the steady state as a linear function of fatigue cycle number N (*SI Appendix*, **Fig. S2**). The energy release rate G, defined as the energy used for fatigue crack growth, is obtained by $G = W(\lambda_{max})H_0$, where $W(\lambda_{max})$ is the area under the loading (W_{ex}) or unloading (W_{el}) curves of the unnotched sample that is cyclically loaded to a steady state when the change in loading-unloading curves becomes negligible (**Fig. 3*A***). Whether the loading or unloading parts should be integrated to obtain $W(\lambda_{max})$ remains controversial (35). We will discuss it in this viscoelastic PA system.

We first show the fatigue-resistant curve of PA-s, that is the plot of $\Delta c/\Delta N$ versus the rescaled energy release rate $\lambda_s^2 G$. **Fig. 3*B*** shows the strong rate dependence of the fatigue-resistance curves. In the large D_i regime where viscoelastic effect exists (D_i= 2.9 and 29, corresponding to lines a and b in **Fig. 2*B***, respectively), multi-mode fatigue resistance occurs, consistent with our previous results (15, 34). That is, a plateau with $\Delta c/\Delta N < 0.1$ μm/cycle is observed at low $\lambda_s^2 G$ above the fatigue threshold, and then $\Delta c/\Delta N$ jumps to several orders of magnitude higher when the $\lambda_s^2 G$ becomes large. The slow fatigue mode is attributed to the presence of a mesoscale bicontinuous phase network structure that suppresses crack propagation above the fatigue threshold (15). While in the small D_i regime where the viscoelastic effect almost diminishes ($D_i = 2.9\times10^{-3}$ and 2.9×10^{-2}, corresponding to lines a' and b' in **Fig. 2*B***, respectively), $\Delta c/\Delta N$ increases rapidly with $\lambda_s^2 G$ above the fatigue threshold, only showing one crack propagation mode. In both regimes, the fatigue-

resistant curves shift to larger $\lambda_s^2 G$ with increasing D_i, suggesting enhancement of fatigue resistance due to increase in viscoelastic dissipation. As expected, the strong viscoelastic regime shows larger discrepancies in the fatigue-resistant curves using the $\lambda_s^2 G$ calculated from W_{ex} and W_{el} than the weak viscoelastic regime.

From the linear plot of $\Delta c/\Delta N$ versus $\lambda_s^2 G$ in **Fig. 3*C***, we obtained the fatigue threshold $\lambda_s^2 G_0$ below which the crack did not grow. In our fatigue test, G_0 was determined below which the crack growth was undetectable with a resolution of 15 μm for N = 50,000 cycles (corresponding to a resolution of 3×10^{-4} μm/cycle). The $\lambda_s^2 G_0$ shows power-law dependence on the D_i, by $\lambda_s^2 G_0 \sim (D_i)^{\upsilon}$, with υ = 0.18 and 0.10 for the $\lambda_s^2 G$ calculated from W_{ex} and W_{el}, respectively (**Fig. 3*D***). This indicates that G_0 calculated from the loading part depends more strongly on the strain rate than that from the unloading part. In the viscoelastic regime, rate dependence of the fatigue threshold is inevitable due to the fast self-healing of broken ionic bonds. Based on the definition of fatigue threshold, i.e., the energy required to fracture a layer of polymer chains, using the unloading curve to calculate the fatigue threshold would be better than the loading curve. By extrapolating the two power-law relations to low strain rate, we get a G_0 value at the intersection where W_{ex}=W_{el} at the steady state of cyclic loading. Since at this condition, no hysteresis exists anymore, the G_0 thus obtained does not contain contribution from ionic bonds and stands for the value in the elastic regime. The intersection value for PA-s is $\lambda_s^2 G_0$ = 27.3 J/m^2 at D_i= 1.35×10^{-3}. We discuss this threshold value later in this paper.

Next, we show the fatigue results for PA-h in **Fig. 4**. In the viscoelastic regime (corresponding to lines a and b in **Fig. 2*D***), a rate dependence of the fatigue resistance is

observed (**Fig. 4*A***). Increasing the D_i, the fatigue resistance curves shift to larger $\lambda_s^2 G$, consistent with the result observed in PA-s. Because a phase separation structure does not form in the water-equilibrated PA-h (15), the homogeneous network and ionic bonds have poor fatigue resistance; thus, $\Delta c/\Delta N$ increases with $\lambda_s^2 G$ by a power law of $\Delta c/\Delta N \sim (\lambda_s^2 G)^5$. The hysteresis loop still exists in the steady state (*SI Appendix*, **Fig. S3*A***), resulting in discrepancies in the fatigue resistance curves for $\lambda_s^2 G$ obtained from W_{ex} and W_{el} (**Fig. 4*A***). In the elastic regime (corresponding to lines a' and b' in **Fig. 2*D***), however, there is no difference between the fatigue resistance curves for $\lambda_s^2 G$ obtained from either W_{ex} or W_{el} because the hysteresis loop no longer exists (*SI Appendix*, **Fig. S3*B***). Moreover, the fatigue resistance curves are rate-independent, and $\Delta c/\Delta N$ increases with $\lambda_s^2 G$ according to the power-law of $\Delta c/\Delta N \sim (\lambda_s^2 G)^{12}$. The two power-law relations of the fatigue-resistant curves in viscoelastic and elastic regimes suggest that the viscoelastic dissipation due to ionic bonds can significantly enhance the crack resistance.

The $\lambda_s^2 G_0$ value of PA-h was obtained from the linear regression of the data in **Fig. 4*A*** on a linear scale (*SI Appendix*, **Fig. S4**). **Fig. 4*B*** shows that the $\lambda_s^2 G_0$ increases slightly with increasing D_i, scaling by the power-law of $\lambda_s^2 G_0 \sim (D_i)^{\upsilon}$ with small values of $\upsilon = 0.10$ and 0.04 for G_0 obtained from W_{ex} and W_{el}, respectively. While the two lines intersect at around $D_i = 0.16$, where the pure elastic behavior is observed by rheology test and tensile test. At $D_i \leqslant 0.16$, $\lambda_s^2 G_0$ is rate-independent. The rate-independent phenomenon has also been observed in hydrogels composed of elastic networks (36).

From the above results, in the viscoelastic regime where mechanical hysteresis exists in the steady state ($W_{ex} > W_{el}$), G_0 has a weak strain rate dependence. Whereas G_0 becomes

rate-independent in the elastic regime. Here, we discuss why the $\lambda_s^2 G_0$ increases with $D_i = 2\pi a_{salt}\dot{\varepsilon}/\omega_v$ in the viscoelastic regime, where hysteresis loops exist in the steady state. The hysteresis loops are derived from the association-disassociation of dynamic bonds due to fast self-healing rate under cyclic fatigue. These repeated debonding and re-bonding of dynamic bonds carry load and dissipate energy, thereby protect the permanent bonds from breaking. We notice that the scaling exponent υ in $\lambda_s^2 G_0 \sim (D_i)^{\upsilon}$ of fatigue test (**Figs. 3*D*** and **4*B***) is much smaller than α in $\lambda_s^2 \Gamma \sim (D_i)^{\alpha}$ of pure shear fracture test (**Fig. 2*F***). The difference could be from three reasons: (1) Different ionic bond density: in fatigue test, only a small fraction of ionic bonds carry load at the steady state, as seen from the shakedown of the hysteresis loop with the increase of cycle (**Fig. 3*A***), while in fracture test, all the ionic bonds carry load and dissipate energy. (2) Different crack propagation rate: crack propagation rate (V_c) in the fracture test is larger than $V_c = 5\times10^4$ μm/s. Given the crack-tip load-transfer length $l = \Gamma/W^* \approx 2$ mm (W^* is the energy density of the unnotched sample stretch up to catastrophic failure (3, 37)), the lowest strain rate at the crack tip is $V_c/l = 25\ s^{-1}$, which means the local loading rate at the crack tip is much larger than the bulk deformation rate. This also may be the reason that fracture energy in the elastic regime follows the same scaling relation as that in viscoelastic regime (**Fig. 2*F***). On the other hand, at the threshold condition of fatigue test, the crack advancing was not observed with a resolution of $\sim10^{-4}$ μm/s. This limit value is 8 decades lower than that in the fracture test. (3) Different stress singularity conditions: based on the birefringence observation, the stress singularity around the crack tip is gradually eliminated with increasing fatigue cycles

in the slow crack propagation mode (15). In contrast, strong stress concentration exists in the fracture test (38).

Finally, we examine if G_0 in the elastic regime could be explained by the Lake–Thomas model (13). In the Lake–Thomas model, G_0 is the energy required to rupture polymer strands lying across the crack plane,

$$G_0 = A\xi\nu_e N_{x,eff} U_b \quad (2)$$

where A is a pre-factor, ξ is the average distance between permanent cross-links, $\xi = \nu_e^{-1/3}$, and U_b is the bond dissociation energy (for a carbon–carbon bond, typically 350 kJ/mol). Substituting the value of ν_e and $N_{x,eff}$ obtained from rheological measurement (**Table 1**), we get G_0 = A × 10.1 and A × 5.1 J/m^2 for PA-s and PA-h, respectively. Intriguingly, considering that one repeating unit of monomer contains two carbon-carbon bonds, taking A = 2 to correct the fracture energy for one strand ($N_{x,eff}U_b$), we obtain a theoretical value of G_0 = 10.2 J/m^2 for PA-h. This value is close to the experiment value of rate-independent $\lambda_s^2 G_0$ (= 9 J/m^2) at the elastic regime (**Fig. 4*B***), consistent with the observation in nearly elastic hydrogels (39, 40). However, a slightly larger value of A = 2.7 is required for PA-s to make the theoretical value of G_0 agree with the experimental value of $\lambda_s^2 G_0$ = 27.3 J/m^2 obtained from the intersection of extrapolation of two power-law relations ($W_{ex} = W_{el}$) in **Fig. 3*D***, where no viscous dissipation is involved in the deformation. A more systematic study on the relationship between the permanent crosslinking structure and G_0 is required in future to quantify the pre-factor A in Eq. 2.

Conclusion

We demonstrated for the first time that the fatigue threshold G_0 is weakly rate-dependent in the viscoelastic regime. Whereas G_0 in the elastic regime is rate-independent and agrees with the predicted value from the Lake–Thomas model. In the viscoelastic regime, the dynamic bonds carry load, protecting the permanent bonds from breaking, and thereby contribute to G_0. Moreover, the fatigue history on dynamic bonds is forgotten due to the self-healing property. By designing dynamic bonds with a relatively long relaxation time so that the observation (working) time window falls in the viscoelastic regime, we can improve the fatigue resistance of soft materials by improving G_0.

In this work, we discussed the physical features of fatigue resistance of self-healing hydrogels with dynamic bonds from linear rheology viewpoint. In the viscoelastic regime, the breaking kinetics of dynamic bonds should depend on the stress/strain being experienced by the dynamic bonds, especially at large deformation. This non-linear rheological effect has been observed in the tensile behaviors of polyampholyte hydrogels (41, 42). How the non-linear rheology effect influences the fatigue behaviors of self-healing materials is unknown. To address this question, studying the fatigue behaviors in the regime $\dot{\varepsilon} >> \tau_s^{-1}$, where the non-linear rheology effect could be mostly prominent, is needed. At such condition, whether the dynamic bonds bring a similar physical effect as that in the short-and long-chain double network materials or not could be clarified. Using self-healing hydrogels with relatively long lifetime of dynamic bonds will allow us to study these behaviors.

Materials and Methods

Sample information

The PA gels used in this work were prepared following the method in ref (6, 43, 44). In short, the precursor solution containing cationic monomer methyl chloride quarternized *N*,*N*-dimethylamino ethylacrylate (DMAEA-Q) and anionic monomer sodium p-styrenesulfonate (NaSS), chemical cross-linker N,N-methylenebis(acrylamide) (MBAA) and 0.1 mol% ultraviolet (UV) initiator α-ketoglutaric acid were randomly polymerized by UV light irradiation. The monomer ratio of NaSS:DMAEA-Q was 0.515:0.485 at the charge balance point. After 11 hours UV light irradiation in an argon atmosphere, the as-prepared gels PA-C_m-C_{MBAA} were obtained, where the C_m is the total monomer concentration and C_{MBAA} is the content of the crosslinker relative to C_m. To investigate the rheology response in varied dynamic regimes, we synthesized one loosely crosslinked PA-2.0-0.1 (denoted as PA-s) and one densely crosslinked PA-2.5-1.0 (denoted as PA-h). The sodium chloride NaCl concentration (C_{salt}) in the as-prepared gels, which is introduced by the counter-ions on the cationic and anionic monomers, are $C_m/2$ = 1.25 and 1.0 M for PA-h and PA-s, respectively. Half of the as-prepared gels were immersed in a large amount of 30 °C deionized water to dialyze for at least one month to remove counter-ions until equilibrium was reached. The deionized water was changed every day. As indicated in our previous work (6), the elemental analysis suggests the water-equilibrated PA-gels prepared at the charge balance point are free of counterions. The water-equilibrated gels exhibit volume shrinking compared with the as-prepared gels due to the electrostatic attraction between the positive and negative charges on the polymer network (18) (**Fig. 1**). The water-equilibrated PA-s and PA-h had a volume shrinkage of 46% and 32%, respectively, compared to the as-prepared state, which gave the relative volume ratio of the as-prepared and water-equilibrated samples λ_s^3 = 1.85 and 1.48 for PA-s and PA-h, respectively. The

polymer volume fractions are ϕ = 0.45 and 0.46 for the equilibrated PA-s and PA-h, respectively.

Rheological test

The dynamic rheological test was performed via an ARES rheometer (advanced rheometric expansion system, Rheometric Scientific Inc.). A disk-shaped sample with diameter 20 mm was fixed between two metal plates. To prevent water evaporating from the gels, the samples were keeping surrounded by water or paraffin oil during the whole procedure of test. The test was performed over a range of angular frequency ω (0.1 to 100 rad/s) at different temperature environment (2 to 82 ℃ for PA-s, and 2 to 62 ℃ for PA-h) at a shear strain of 0.1 %. The dynamic behavior of the PA gels at different temperatures and frequencies was verified to following the time-temperature superposition in ref (6). By following the principle of time-temperature superposition, master curves of storage modulus (G'), loss modulus (G'') and loss factor tan δ were constructed at a reference temperature of 24 ℃. Time-salt superposition principle was applied to construct the master curves of frequency sweep of the salt-containing and salt-free gels.

The effective permanent cross-linker densities v_e and the number of monomers per network strands $N_{x,eff}$ of the gels were estimated from the dynamic shear modulus G' in the plateau regime at low frequency, where the contribution of ionic bonds is negligible, using the relation,

$$G' = v_e k_B T = \frac{\rho \phi N_A k_B T}{M_0 N_{x,eff}} \quad (3)$$

where k_B and T are Boltzmann constant (1.38×10^{-23} J/K) and the absolute temperature (297.15 K), respectively. The ρ is dry polymer density (1.4×10^{6} g/m^3). M_0 and N_A are the molecular weight of the monomer without counterions (170.7 g/mol) and Avogadro constant (6.02×10^{23} /mol), respectively. Eq. 3 assumes that effective cross-links move affinely in response to small oscillation amplitudes of shear. The ν_e and $N_{x,eff}$ stand for the permanent crosslinking from the chemical crosslinker and the trapped entanglements (18).

For PA-h, we got the modulus G' = 71 kPa from the plateau at low frequency of the master curve in **Fig. 2*D***. For PA-s, a frequency-independent G' was not accessible in our observation scale, so we took the value G' = 8.44 kPa at the lowest frequency on the master curve (**Fig. 2*B***). The obtained ν_e and $N_{x,eff}$ for the two gels are shown in **Table 1**.

Pure shear and fatigue tests

Both the as-prepared gels with the presence of high concentration small counter-ions (Na^+ and Cl^-) and water-equilibrated gels with negligible small ions Na^+ and Cl^- were used to investigate the relations between dynamic response and mechanical properties. The gels in the water-equilibrated state were taken as the reference state in all the experiments. Taking the length swelling ratio of the undeformed water-equilibrated gels as 1, the relative length swelling ratio of undeformed as-prepared gels is λ_s (**Fig. 1**). Pure shear test was used to characterize the toughness of the gels, and cyclic loading was used for fatigue test using sample with the pure shear geometry (**Fig. 2*E***). The nominal strain rates of $\dot{\varepsilon}= v/H_0$=0.25 s^{-1} and 2.5 s^{-1} were applied, where v is the loading speed and H_0 is the initial sample height. All of the pure shear and fatigue tests were performed at room temperature. To prevent the sample from dehydrating during the test, we kept the water-equilibrated gels in the water

vapor atmosphere during the test as shown in (34), and the as-prepared gels were smeared silicone oil on the surface layers. The stress (σ)-stretch (λ) curves were recorded during the pure shear and fatigue tests, where σ is force over the initial undeformed cross-sectional area, λ is the ratio between the deformed sample height and the initial sample height. The method to use σ - λ curves to obtain fracture energy (Γ) and energy release rate (G) are shown in *SI Appendix*, **Fig. S1** and **Fig. 3*A***, respectively.

Data Availability. All data are included in the main text and SI Appendix.

Acknowledgments

The authors gratefully acknowledge support from Japan Society for the Promotion of Science KAKENHI (Grant no. JP17H06144).

References

1. J. Slootman, V. Waltz, C. J. Yeh, C. Baumann, R. Göstl, J. Comtet, C. Creton, Quantifying rate- and temperature-dependent molecular damage in elastomer fracture. *Phys. Rev. X* **10**, 041045 (2020).
2. L. Chen, T. L. Sun, K. Cui, D. R. King, T. Kurokawa, Y. Saruwatari, J. P. Gong, Facile synthesis of novel elastomers with tunable dynamics for toughness, self-healing and adhesion. *J. Mater. Chem. A* **7**, 17334-17344 (2019).
3. R. Long, C.-Y. Hui, J. P. Gong, E. Bouchbinder, The fracture of highly deformable soft materials: A tale of two length scales. *Annu. Rev. Condens. Matter Phys.* **12**, 71-94 (2020).
4. E. Filippidi, T. R. Cristiani, C. D. Eisenbach, J. H. Waite, J. N. Israelachvili, B. K. Ahn, M. T. Valentine, Toughening elastomers using mussel-inspired iron-catechol complexes. *Science* **358**, 502-505 (2017).
5. S. P. O. Danielsen, H. K. Beech, S. Wang, B. M. El-Zaatari, X. Wang, L. Sapir, T. Ouchi, Z. Wang, P. N. Johnson, Y. Hu, D. J. Lundberg, G. Stoychev, S. L. Craig, J. A. Johnson, J. A. Kalow, B. D. Olsen, M. Rubinstein, Molecular characterization of polymer networks. *Chem. Rev.* **121**, 5042-5092 (2021).
6. T. L. Sun, T. Kurokawa, S. Kuroda, A. B. Ihsan, T. Akasaki, K. Sato, M. A. Haque, T. Nakajima, J. P. Gong, Physical hydrogels composed of polyampholytes demonstrate high toughness and viscoelasticity. *Nat. Mater.* **12**, 932-937 (2013).

7. C. Du, X. N. Zhang, T. L. Sun, M. Du, Q. Zheng, Z. L. Wu, Hydrogen-bond association-mediated dynamics and viscoelastic properties of tough supramolecular hydrogels. *Macromolecules* **54**, 4313-4325 (2021).
8. D. C. Taylor, J. D. Dalton JR, A. V. Seaber, W. E. Garrett JR, Viscoelastic properties of muscle-tendon units: the biomechanical effects of stretching. *Am. J. Sports Med.* **18**, 300-309 (1990).
9. J. L. Gennisson, T. Deffieux, E. Mace, G. Montaldo, M. Fink, M. Tanter, Viscoelastic and anisotropic mechanical properties of in vivo muscle tissue assessed by supersonic shear imaging. *Ultrasound Med. Biol.* **36**, 789-801 (2010).
10. R. Bai, J. Yang, Z. Suo, Fatigue of hydrogels. *Eur. J. Mech. A/Solids* **74**, 337-370 (2019).
11. R. Bai, J. Yang, X. P. Morelle, C. Yang, Z. Suo, Fatigue fracture of self-recovery hydrogels. *ACS Macro Lett.* **7**, 312-317 (2018).
12. G. Lake, Fatigue and fracture of elastomers. *Rubber Chem. Technol.* **68**, 435-460 (1995).
13. G. Lake, A. Thomas, The strength of highly elastic materials. *Proc. R. Soc. London A* **300**, 108-119 (1967).
14. W. Zhang, J. Hu, J. Tang, Z. Wang, J. Wang, T. Lu, Z. Suo, Fracture toughness and fatigue threshold of tough hydrogels. *ACS Macro Lett.* **8**, 17-23 (2018).
15. X. Li, K. Cui, T. Kurokawa, Y. N. Ye, T. L. Sun, C. Yu, C. Creton, J. P. Gong, Effect of mesoscale phase contrast on fatigue-delaying behavior of self-healing hydrogels. *Sci. Adv.* **7**, eabe8210 (2021).
16. G. Scetta, N. Selles, P. Heuillet, M. Ciccotti, C. Creton, Cyclic fatigue failure of TPU using a crack propagation approach. *Polym. Test.* **97**, 107140 (2021).
17. T. L. Sun, F. Luo, T. Kurokawa, S. N. Karobi, T. Nakajima, J. P. Gong, Molecular structure of self-healing polyampholyte hydrogels analyzed from tensile behaviors. *Soft matter* **11**, 9355-9366 (2015).
18. K. Cui, Y. N. Ye, T. L. Sun, C. Yu, X. Li, T. Kurokawa, J. P. Gong, Phase separation behavior in tough and self-healing polyampholyte hydrogels. *Macromolecules* **53**, 5116-5126 (2020).
19. A. V. Dobrynin, R. H. Colby, M. Rubinstein, Scaling theory of polyelectrolyte solutions. *Macromolecules* **28**, 1859-1871 (1995).
20. A. V. Dobrynin, M. Rubinstein, Theory of polyelectrolytes in solutions and at surfaces. *Prog. Polym. Sci.* **30**, 1049-1118 (2005).
21. J. D. Ferry, *Viscoelastic properties of polymers*. (John Wiley & Sons, New York, 1980), 3rd ed.
22. H. M. Wyss, K. Miyazaki, J. Mattsson, Z. Hu, D. R. Reichman, D. A. Weitz, Strain-rate frequency superposition: a rheological probe of structural relaxation in soft materials. *Phys. Rev. Lett.* **98**, 238303 (2007).
23. E. Spruijt, J. Sprakel, M. Lemmers, M. A. Stuart, J. van der Gucht, Relaxation dynamics at different time scales in electrostatic complexes: time-salt superposition. *Phys. Rev. Lett.* **105**, 208301 (2010).
24. S. Ali, V. M. Prabhu, Relaxation behavior by time-salt and time-temperature superpositions of polyelectrolyte complexes from coacervate to precipitate. *Gels* **4**, 11 (2018).
25. Z. Zhang, Q. Chen, R. H. Colby, Dynamics of associative polymers. *Soft Matter* **14**, 2961-2977 (2018).
26. Q. Chen, Z. Zhang, R. H. Colby, Viscoelasticity of entangled random polystyrene ionomers. *J. Rheol.* **60**, 1031-1040 (2016).
27. M. Rubinstein, R. H. Colby, *Polymer Physics*. (Oxford University Press, New York, 2003).
28. J. Kim, G. Zhang, M. Shi, Z. Suo, Fracture, fatigue, and friction of polymers in which entanglements greatly outnumber cross-links. *Science* **374**, 212-216 (2021).
29. D. Zheng, S. Lin, J. Ni, X. Zhao, Fracture and fatigue of entangled and unentangled polymer networks. *Extreme Mech. Lett.* **51**, 101608 (2022).

30. R. Long, C.-Y. Hui, Fracture toughness of hydrogels: measurement and interpretation. *Soft Matter* **12**, 8069-8086 (2016).
31. J.-Y. Sun, X. Zhao, W. R. Illeperuma, O. Chaudhuri, K. H. Oh, D. J. Mooney, J. J. Vlassak, Z. Suo, Highly stretchable and tough hydrogels. *Nature* **489**, 133–136 (2012).
32. O. H. Yeoh, Analysis of deformation and fracture of 'pure shear' rubber testpiece. *Plastics, Rubber and Composites* **30**, 389-397 (2013).
33. F. Luo, T. L. Sun, T. Nakajima, T. Kurokawa, Y. Zhao, A. B. Ihsan, H. L. Guo, X. F. Li, J. P. Gong, Crack blunting and advancing behaviors of tough and self-healing polyampholyte hydrogel. *Macromolecules* **47**, 6037-6046 (2014).
34. X. Li, K. Cui, T. L. Sun, L. Meng, C. Yu, L. Li, C. Creton, T. Kurokawa, J. P. Gong, Mesoscale bicontinuous networks in self-healing hydrogels delay fatigue fracture. *Proc. Natl. Acad. Sci. U.S.A.* **117**, 7606-7612 (2020).
35. R. Bai, Q. Yang, J. Tang, X. P. Morelle, J. Vlassak, Z. Suo, Fatigue fracture of tough hydrogels. *Extreme Mech. Lett.* **15**, 91-96 (2017).
36. S. Lin, J. Ni, D. Zheng, X. Zhao, Fracture and fatigue of ideal polymer networks. *Extreme Mech. Lett.* **48**, 101399 (2021).
37. C. Chen, Z. Wang, Z. Suo, Flaw sensitivity of highly stretchable materials. *Extreme Mech. Lett.* **10**, 50-57 (2017).
38. T. L. Sun, F. Luo, W. Hong, K. Cui, Y. Huang, H. J. Zhang, D. R. King, T. Kurokawa, T. Nakajima, J. P. Gong, Bulk energy dissipation mechanism for the fracture of tough and self-healing Hydrogels. *Macromolecules* **50**, 2923-2931 (2017).
39. E. Zhang, R. Bai, X. P. Morelle, Z. Suo, Fatigue fracture of nearly elastic hydrogels. *Soft matter* **14**, 3563-3571 (2018).
40. Y. Zhou, W. Zhang, J. Hu, J. Tang, C. Jin, Z. Suo, T. Lu, The stiffness-threshold conflict in polymer networks and a resolution. *J. Appl. Mech.* **87**, 031002 (2020).
41. S. P. Venkata, K. Cui, J. Guo, A. T. Zehnder, J. P. Gong, C.-Y. Hui, Constitutive modeling of bond breaking and healing kinetics of physical Polyampholyte (PA) gel. *Extreme Mech. Lett.* **43**, 101184 (2021).
42. K. Cui, J. P. Gong, How double dynamics affects large deformation and fracture of soft materials. *J. Rheol.* **In press**, (2022).
43. A. B. Ihsan, T. L. Sun, T. Kurokawa, S. N. Karobi, T. Nakajima, T. Nonoyama, C. K. Roy, F. Luo, J. P. Gong, Self-healing behaviors of tough polyampholyte hydrogels. *Macromolecules* **49**, 4245-4252 (2016).
44. A. B. Ihsan, T. L. Sun, S. Kuroda, M. A. Haque, T. Kurokawa, T. Nakajima, J. P. Gong, A phase diagram of neutral polyampholyte–from solution to tough hydrogel. *J. Mater. Chem. B* **1**, 4555-4562 (2013).

Figures and Tables

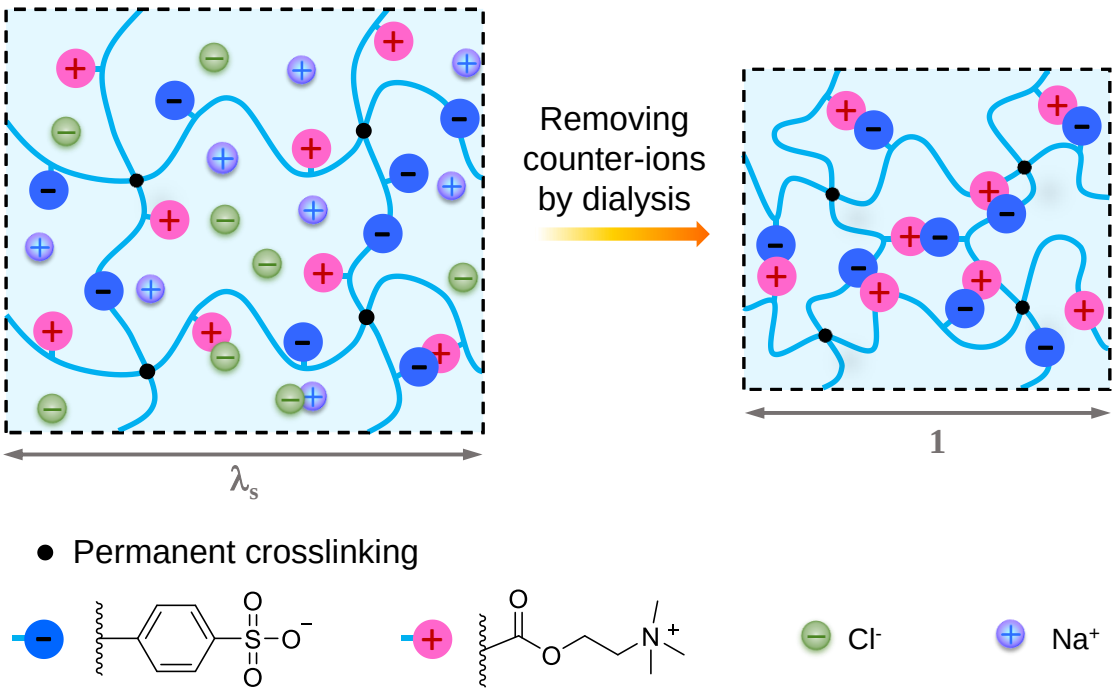

Fig. 1. Schematic illustration of switch off/on of the dynamic bonds on polyampholyte network. The dynamic bonds are switched off in the as-prepared gels with counter-ions (left). The dynamic bonds are switched on when the counter-ions are dialyzed in deionized water to equilibrated state, and the water-equilibrated gels shrink owing to the ionic bonding between the oppositive charges on polyampholyte network (right). Taking the undeformed water-equilibrated gels as reference state (length swelling ratio = 1), the relative length swelling ratio of undeformed as-prepared gel is λ_s due to volume difference.

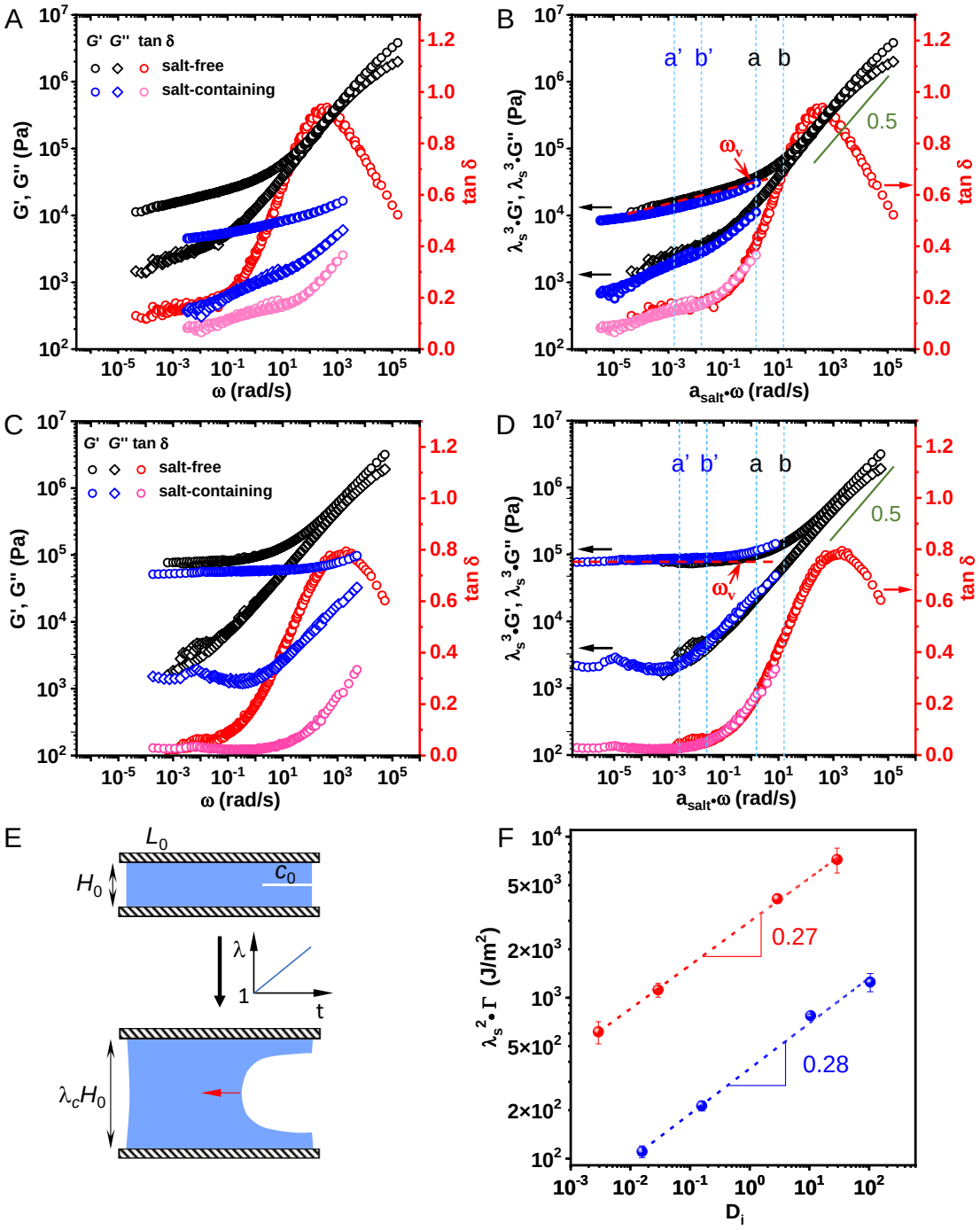

Fig. 2. Constructed master curves of mechanical properties of PA gels through time–salt superposition. (***A***) Frequency sweep curves of the salt-containing and salt-free PA-s by time-temperature superposition at a reference temperature of 24 °C. (***B***) The master curves of frequency sweep constructed from time–salt superposition for PA-s using the curves in (*A*). (***C***) Frequency sweep curves of the salt-containing and salt-free PA-h by time-temperature superposition at a reference temperature of 24 °C. (***D***) The master curves

of frequency sweep constructed from time–salt superposition for PA-h using the curves in (*C*). For time–salt superposition, salt-free state is taken as the reference state, and the shift factor a_{salt} for frequency is shown in **Table 2**. The storage modulus *G*' and loss modulus *G*'' of the salt-containing gels are rescaled by volume change ratio λ_s^3 due to polymer density difference in per unit volume. Vertical dotted lines in (*B*) and (*D*) indicate the equivalent angular frequencies $a_{salt}\omega = 2\pi a_{salt}\dot{\varepsilon}$ for the measurements at strain rate $\dot{\varepsilon} = 0.25$ s^{-1} (a') and 2.5 s^{-1} (b') for the salt-containing gels, and $\dot{\varepsilon} = 0.25$ s^{-1} (a) and 2.5 s^{-1} (b) for the salt-free gels. The ω_v is the transition angular frequency from plateau regime to the viscoelastic regime. (***E***) Pure shear test and the geometry (L_0 = 50 mm, H_0 = 10 mm, and c_0 = 10 mm) used for characterizing toughness (Γ). (***F***) The rescaled toughness $\lambda_s^2\Gamma$ against the dimensionless quantity, $D_i = 2\pi a_{salt}\dot{\varepsilon}/\omega_v$. D_i denotes the observation strain rate in relative to the longest viscoelastic relaxation rate ω_v. red sphere: PA-s, blue sphere: PA-h. Data in (*F*) are means ± SD, n = 3.

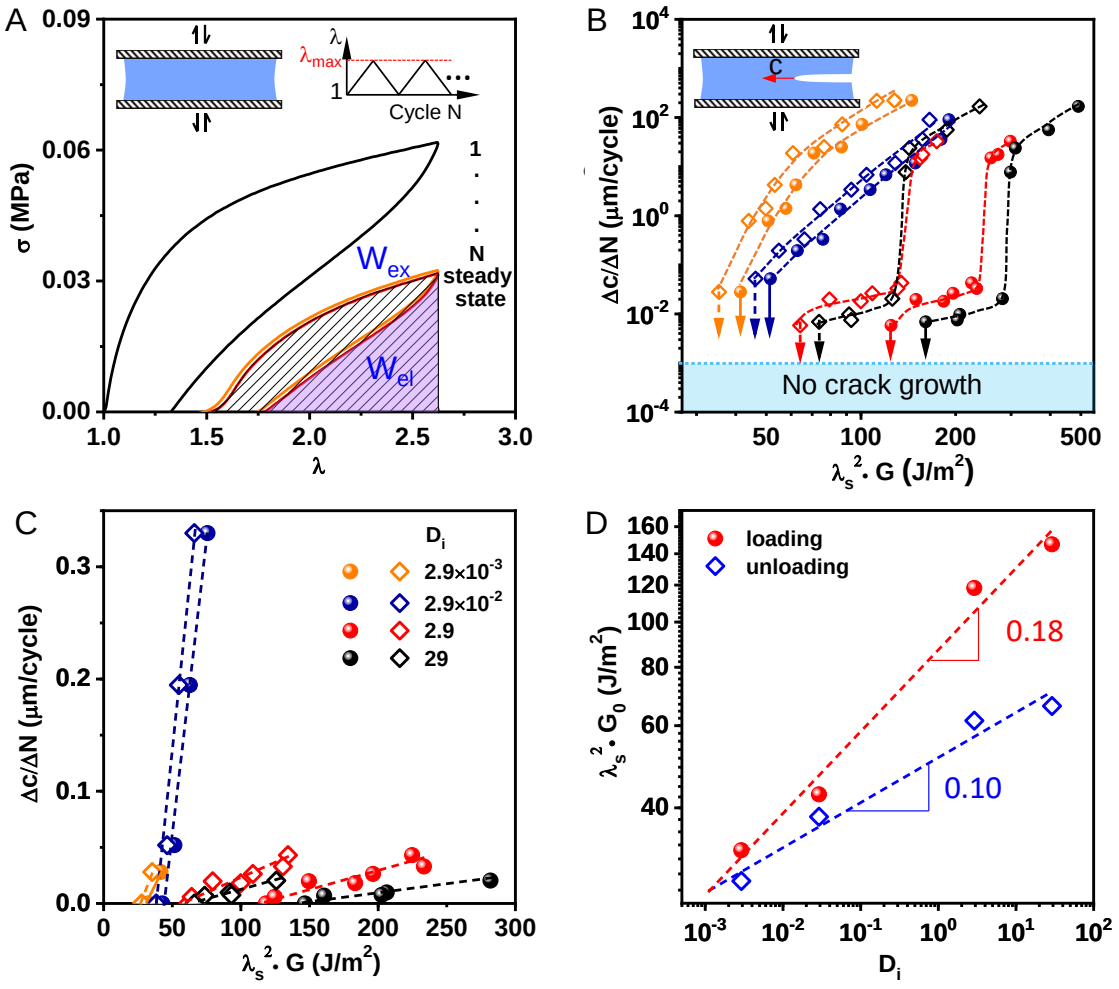

Fig. 3. Fatigue behavior of the loosely crosslinked PA-s in a broad $D_i = 2\pi a_{salt}\dot{\varepsilon}/\omega_v$. (***A***) The shakedown process of stress (σ)–stretch (λ) curve of unnotched sample in cyclic loading (inset), and the energy density in loading part W_{ex} (area in hatch lines) and unloading W_{el} (area in light purple) in the steady state are used for calculating energy release rate G. (***B*** and ***C***) The crack growth per cycle ($\Delta c/\Delta N$) as a function of rescaled energy release rate ($\lambda_s^2 G$) obtained from the W_{ex} (spheres) and W_{el} (diamonds) in logarithmic scale (***B***) and initial linear regime in the linear scale (***C***). Symbols in (*B*) are the same as those in (*C*). Dashed curves (lines) are guides for the eyes. (***D***) The fatigue threshold $\lambda_s^2 G_0$ as a function of D_i. Red sphere: G_0 obtained from W_{ex}, blue diamond: G_0 obtained from W_{el}. Dashed lines are fitted power-law relations and their extrapolations to low D_i.

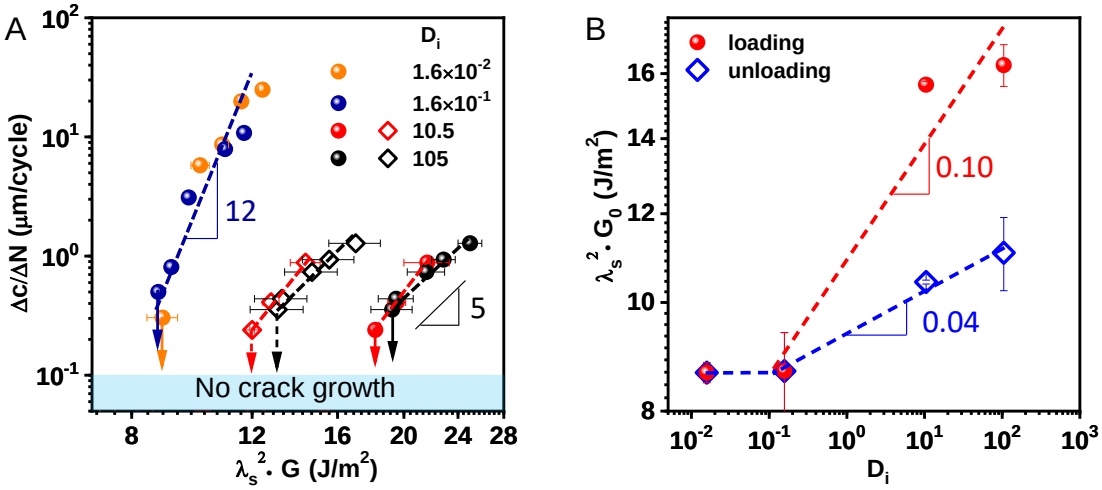

Fig. 4. Fatigue behavior of the densely crosslinked PA-h. (***A***) The crack growth per cycle $\Delta c/\Delta N$ versus rescaled energy release rate $\lambda_s^2 G$ obtained from the W_{ex} (spheres) and W_{el} (diamonds). (***B***) The fatigue threshold $\lambda_s^2 G_0$ versus $D_i = 2\pi a_{salt}\dot{\varepsilon}/\omega_v$. Red sphere: G_0 obtained from W_{ex}, blue diamond: G_0 obtained from W_{el}. The error bars are SDs due to the strain fluctuations of tensile machine in a small range.

Table 1. Sample formulations and obtained structures at water-equilibrated state.

	Total monomer concentration C_m (M)	Crosslinker density C_{MBAA} (mol%)	Permanent crosslinking density, ν_e (m^{-3})	Number of monomers per strand, $N_{x,eff}$
PA-s	2.0	0.1	2.1×10^{24}	1080
PA-h	2.5	1.0	1.7×10^{25}	130

Table 2. Shift factors used for rescaling the storage modulus (G') and loss modulus (G'') of as-prepared PA gels containing salt into the data of water-equilibrated PA gels (salt-free) in **Fig. 2**. The C_{salt} is the NaCl concentration in the as-prepared gel introduced by the counter-ions on the cationic and anionic monomers.

	$C_{salt} = C_m/2$ (M)	a_{salt}	$b_{salt} = \lambda_s^3$
PA-s	1.0	0.001	1.85
PA-h	1.25	0.0015	1.48

PNAS
www.pnas.org

Supplementary Information for

Role of dynamic bonds on fatigue threshold of tough hydrogels

Xueyu Li and Jian Ping Gong

*Jian Ping Gong

Email: gong@sci.hokudai.ac.jp

This PDF file includes:

Figs S1 to S4

SI References

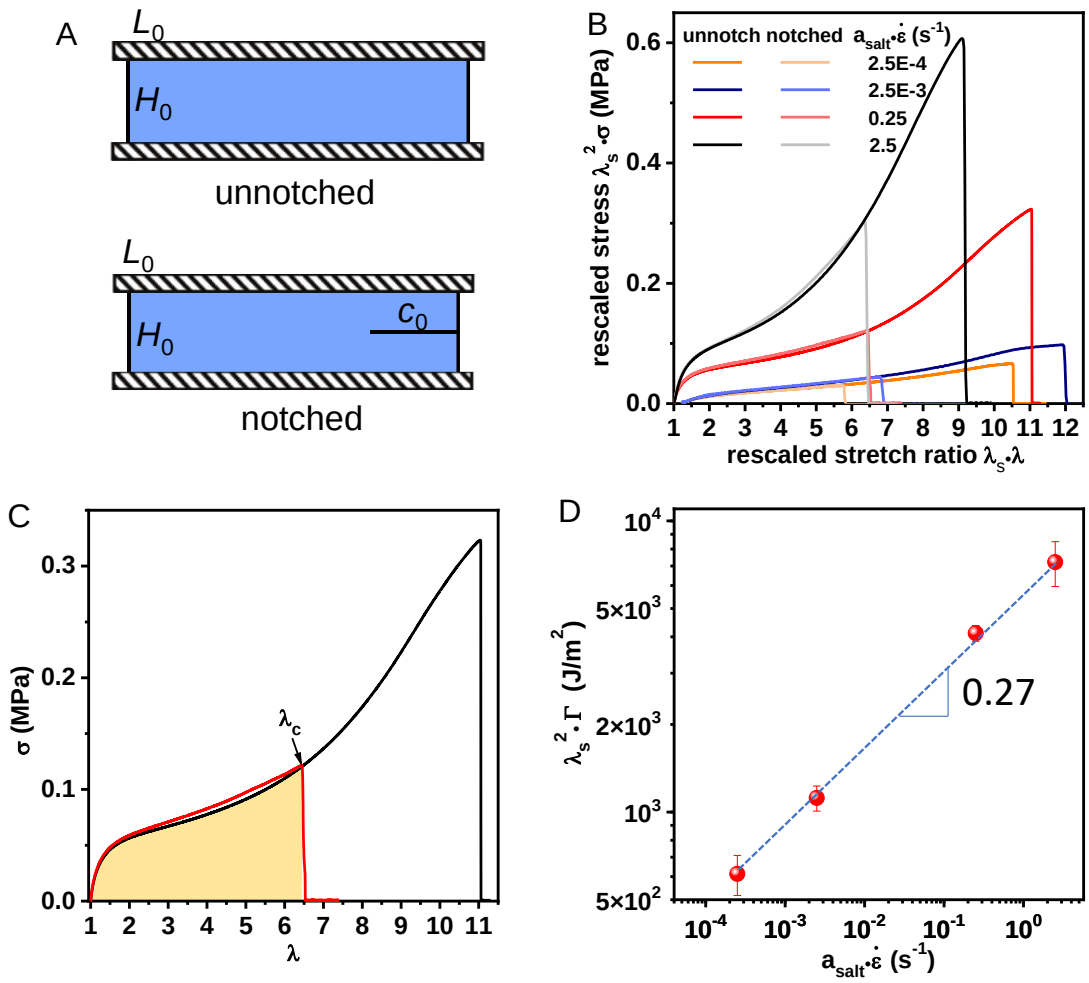

Fig. S1. Method to get fracture energy of PA gels by pure shear test. The loosely crosslinked PA-s is taken as an example. (***A***) The geometry of unnotched and notched samples applied in the pure shear test (L_0 = 50 mm, H_0 = 10 mm, and c_0 = 10 mm). (***B***) The rescaled stress $\lambda_s^2\sigma$ as a function of rescaled stretch ratio $\lambda_s\lambda$ in the pure shear test at varied equivalent strain rates ($a_{salt}\dot{\varepsilon}$). The σ is force over the initial undeformed cross-sectional area, λ is the ratio between the deformed sample height and the initial sample height, and λ_s is the length ratio of the as-prepared PA gels in relative to the water-equilibrated gels (**Fig. 1**). The σ of notched sample has been corrected by the effective initial area of cross section. (***C***) An example to get the fracture energy. The fracture energy is calculated from $\Gamma=W(\lambda_c)H_0$, where $W(\lambda_c)$ is the energy density of the unnotched sample stretch to λ_c (area in yellow), and H_0 is the sample height when undeformed, λ_c is the critical stretch ratio for crack starting to propagate. The integrated area under the σ - λ curve up to catastrophic failure of the unnotched sample is denoted as W^*, which is used to calculate the crack-tip load-transfer length l by $l = \Gamma/W^*$ (1, 2). (***D***) The rescaled fracture energy $\lambda_s^2\Gamma$ versus equivalent strain rate $a_{salt}\dot{\varepsilon}$ for PA-s.

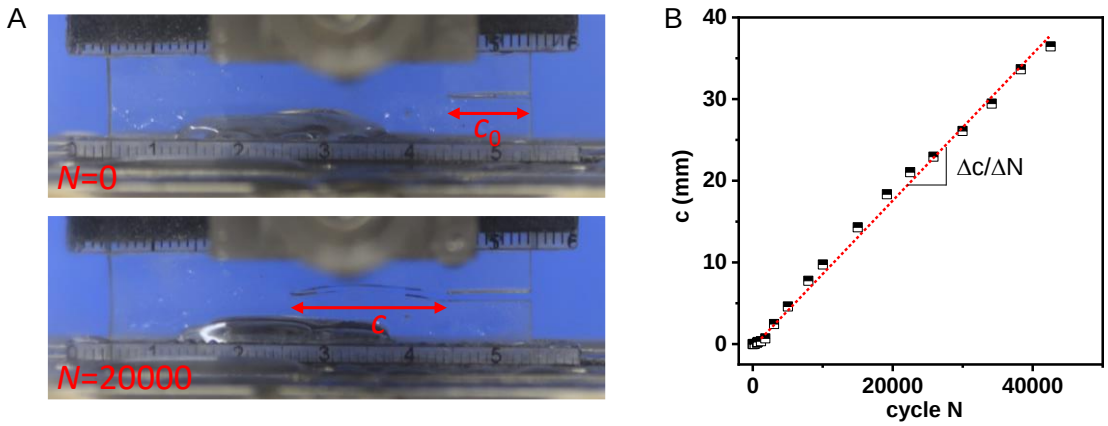

Fig. S2. Method to get fatigue crack growth per cycle (Δ*c*/Δ*N*). (***A***) Photos of crack propagation in fatigue test. The water-equilibrated PA-h tested at λ_{max}=1.16 under $\dot{\varepsilon}$=0.25 s^{-1} is taken as an example. The crack growth *c* is plotted as a function of cycle number *N* as shown in (*B*). (***B***) The method to obtain the crack growth per cycle (Δ*c*/Δ*N*), by fitting slope of *c* in the steady state as a linear function of fatigue cycle number *N*.

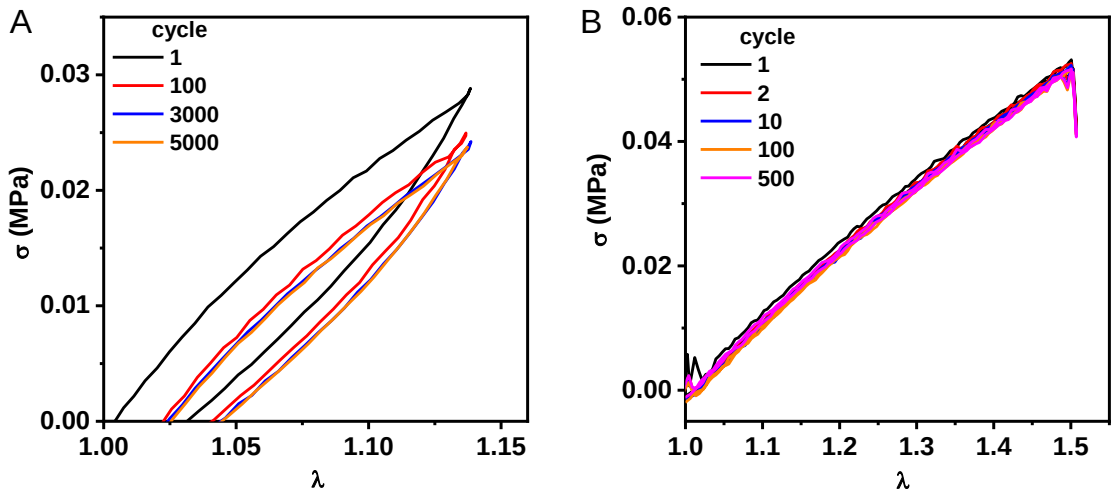

Fig. S3. Stress (σ)-stretch (λ) curve of unnotched PA-h. (***A***) The water-equilibrated PA-h cyclic loading at λ_{max}=1.14 under $\dot{\varepsilon}$=0.25 s^{-1} ($D_i = 2\pi a_{salt}\dot{\varepsilon}/\omega_v = 10.5$). (***B***) The as-prepared PA-h cyclic loading at λ_{max}=1.5 under $\dot{\varepsilon}$=0.25 s^{-1}($D_i = 2\pi a_{salt}\dot{\varepsilon}/\omega_v = 1.6 \times 10^{-2}$).

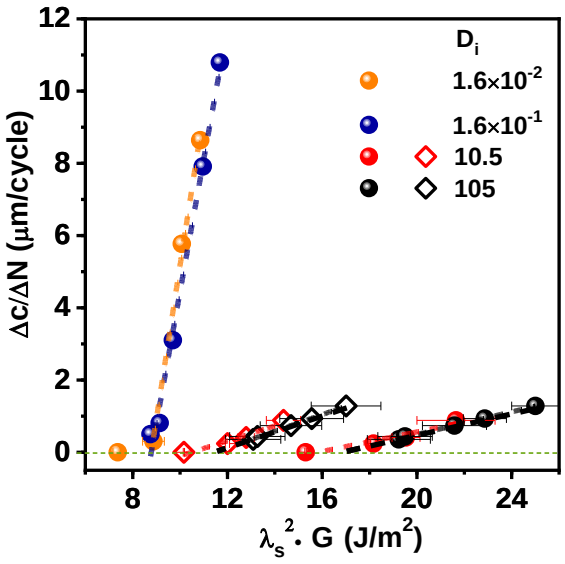

Fig. S4. The crack growth per cycle ($\Delta c/\Delta N$) as a function of rescaled energy release rate ($\lambda_s^2 G$) obtained from the W_{ex} (spheres) and W_{el} (diamonds) in initial linear regime in the linear scale of PA-h. For $D_i \leq 0.16$, PA-h becomes pure elastic and we have $W_{ex}=W_{el}$. The G_0 of PA-h was obtained from the intercept of the curve on the $\lambda_s^2 G$ axis when $\Delta c/\Delta N=0$ through linear regression.

SI References

1. C. Chen, Z. Wang, Z. Suo, Flaw sensitivity of highly stretchable materials. *Extreme Mech. Lett.* **10**, 50-57 (2017).
2. R. Long, C.-Y. Hui, J. P. Gong, E. Bouchbinder, The fracture of highly deformable soft materials: A tale of two length scales. *Annu. Rev. Condens. Matter Phys.* **12**, 71-94 (2020).